

# Ultra-stable Imine-based Covalent Organic Frameworks: An Effect of Interlayer Hydrogen Bonding

Arjun Halder,<sup>a,b</sup> Suwendu Karak,<sup>a,b</sup> Matthew Addicoat,<sup>c</sup> Saibal Bera,<sup>a,b</sup> Shebeeb Kunjattu H.,<sup>c</sup> Pradip Pachfule,<sup>a,b</sup> Thomas Heine,<sup>d</sup> Ulhas K. Kharul<sup>e</sup> and Rahul Banerjee<sup>\*b,e</sup>

<sup>a</sup>Academy of Scientific and Innovative Research (AcSIR), CSIR-National Chemical Laboratory, Dr. Homi Bhabha Road, Pune-411 008, India.

<sup>b</sup>Physical/Materials Chemistry Division, CSIR-National Chemical Laboratory, Dr. Homi Bhabha Road, Pune-411 008, India.

<sup>c</sup>Polymer Science and Engineering Division, CSIR-National Chemical Laboratory, Pune 411008, India.

<sup>d</sup>Center for Functional Nanomaterials, School of Engineering and Science, Jacobs University Bremen, Research III, Room 61, Campus Ring 1, 28759 Bremen, Germany.

<sup>e</sup>Department of Chemical Sciences, Indian Institute of Science Education and Research (IISER) Kolkata, Mohanpur Campus, Mohanpur, 741252 (India).

<sup>\*</sup>School of Science and Technology, Nottingham Trent University, Clifton Lane, NG11 8NS Nottingham, United Kingdom.

**ABSTRACT:** Covalent Organic Frameworks (COFs) have convened inordinate scientific attention from last few years because of their unique tunable porosity and long range ordered structures with high atomic precisions. Although the high crystalline nature with considerable porosity fashioned these novel materials as an eligible candidate for diverse applications, the ordered nano-channels with controllable pore aperture, especially regarding membrane separations in extreme conditions, have been poorly explored. Herein, we have demonstrated rapid and scalable synthesis of six new imine-linked highly crystalline and porous COFs *via* salt (*p*-toluenesulfonic acid) mediated solid state crystallization approach. These as-synthesized materials show exceptionally high chemical stability in harsh environments including conc. H<sub>2</sub>SO<sub>4</sub> (36 N), conc. HCl (12 N) and NaOH (9N). This is exclusively because of the presence of strong interlayer C–H...N H-bonding interactions among the individual layers. This H-bonding reinforce interlayer stacking interaction and provides a steric hindrance and hydrophobic environment around the imine (–C=N) bonds making it safe from hydrolysis, as confirmed by ~~the~~ Density Functional Theory (DFT) calculations. By taking advantage of processability of COF powders in salt mediated synthesis approach, the continuous, porous, crystalline, self-standing and crack-free COF membranes (COFMs) with high chemical stability have been transmuted, for their potential applications to separate various environmentally toxic materials from drinking water with high water flux. Moreover, owing to its highly robust backbone, the COFM have showed ~~the~~ unprecedented Sulfuric acid (12 N) permeance reflecting its potential applications for sulfuric acid purification. Also, the as-synthesized COFMs exhibit exceptionally high permeance of acetonitrile (380 Lm<sup>2</sup>h<sup>−1</sup>bar<sup>−1</sup>) and acetone (340 Lm<sup>2</sup>h<sup>−1</sup>bar<sup>−1</sup>).

## Introduction

Covalent Organic Frameworks (COFs) are pristine sets of covalently linked periodically ordered two or three-dimensional (2D/3D) porous networks contrived through simultaneous polymerization and crystallization of monomeric building blocks.<sup>1</sup> The crystallization process of such structurally predesigned organic porous structures require dynamic reversible bond formation, like boronic acid trimerization, boronate ester formation, Schiff base formation, etc.<sup>2</sup> However, the reversible nature of these chemical bonds imparts a limit towards their chemical stability and creates a restriction towards the usage of these novel materials for expansive utilizations.<sup>3</sup> Hence, the design and synthesis of porous crystalline COFs, which can sustain their crystallinity and porosity in abrasive environments including drastic humidity, strong acidity or basicity, is still a key challenge for the modern researchers.<sup>4</sup>

We have already attempted to overcome this stability issues in COFs, by introducing the enol to keto tautomerization phenomenon during the framework crystallization. By using this approach, we could achieve a set of COFs with significantly enhanced chemical (aqueous, acid and base) stability.<sup>4a, 5</sup> However, this idea is entirely restricted to  $\beta$ -keto-enamine COFs, which provides minimal substrate scope, limiting its widespread exploration. Hence, it is necessary to diversify this approach and extend this idea for the production of more versatile “–C=N” (imine) linked COFs. The exploration of imine-linked COFs has increased dramatically in recent years owing to the superior hydrolytic stability compared to boronic acid COFs along with extensive substrate-library availability.<sup>6</sup> However, for the widespread implementation of such chemically stable imine based COFs, the synthetic process should: 1) be a greener approach of synthesis i.e. devoid of toxic solvents or synthetic difficulty,<sup>5b, 7a, 2</sup> be rapid and easily scalable (unlike the traditional solvothermal process),<sup>5b, 7b</sup> and 3) provide the opportunity to process the as-synthesized COFs into pallets,

beads as well as membranes keeping their ~~property-properties~~ intact.<sup>5a, 5b</sup>

Keeping all these in perspective, herein, we introduce 2,4,6-trimethoxy-1,3,5-benzenetricarbaldehyde (TpOMe) as a prime

aldehyde building unit for scalable and rapid construction of chemically

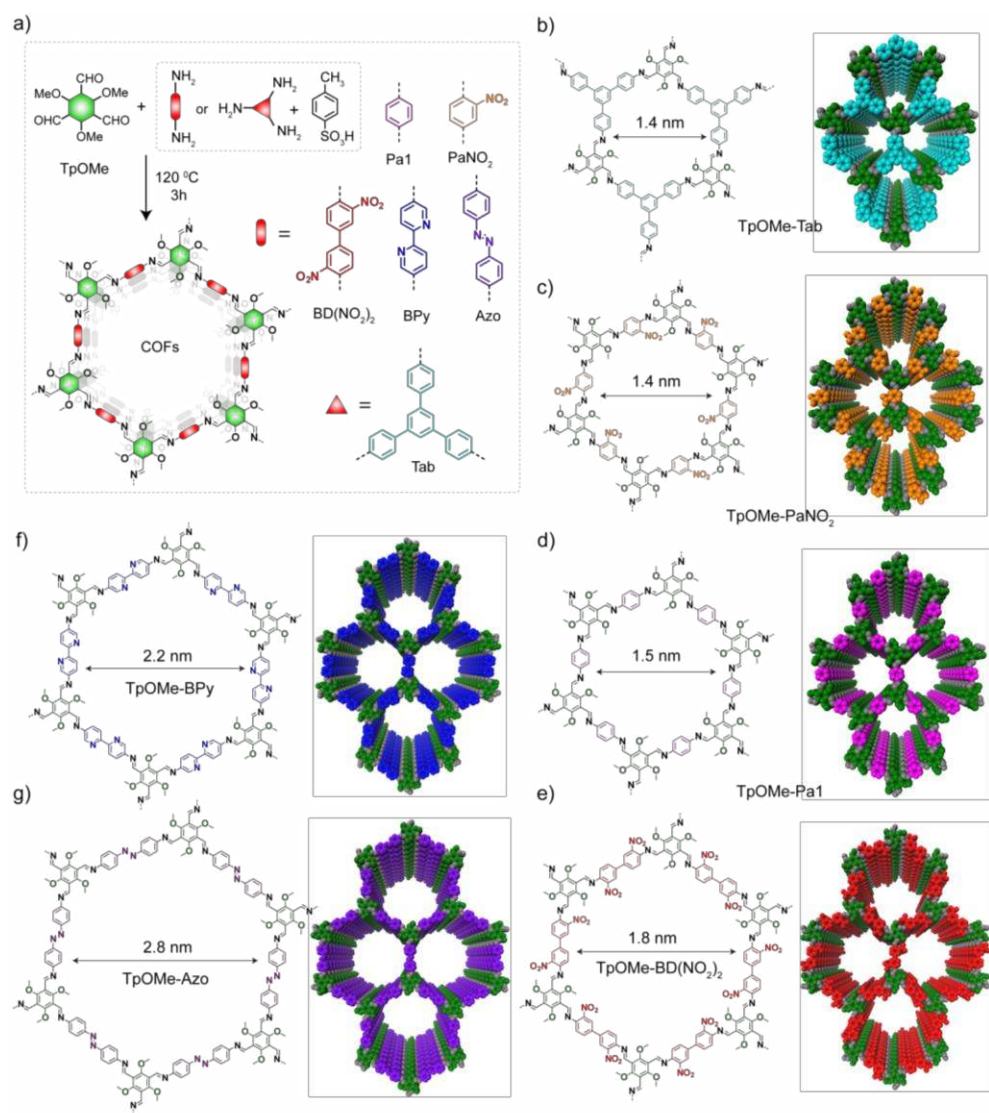


**Figure 1.** (a) General representation for the synthesis of six COFs from aldehyde (TpOMe) and corresponding amines (Tab, PaNO<sub>2</sub>, Pa1, BD(NO<sub>2</sub>)<sub>2</sub>, BPy and Azo) by PTSA (*p*-toluenesulfonic acid) mediated Schiff base reaction. (b-g) Chem. draw structures of TpOMe-Tab, TpOMe-PaNO<sub>2</sub>, TpOMe-Pa1, TpOMe-BD(NO<sub>2</sub>)<sub>2</sub>, TpOMe-BPy and TpOMe-Azo, with their corresponding eclipsed (AA stacked) space filling models. The experimental pore diameters of the hexagonal COFs have been shown with double headed arrow within the drawings.

stable imine-linked COFs *via* PTSA (*p*-toluenesulfonic acid) mediated solid-state mixing approach.<sup>5b</sup> Introduction of three bulky methoxy (–OCH<sub>3</sub>) groups adjacent to the aldehyde (–CHO) functionalities provide significant steric hindrance and the hydrophobic environment around the imine bonds, promoting impregnable COF crystallization. These as-synthesized materials showcase exceptionally high chemical stability in H<sub>2</sub>SO<sub>4</sub> (36 N), HCl (12N), NaOH (9 N), boiling water and common organic solvents, for

several days. To the best of our knowledge, this is the first report that illustrates a series of imine based COFs with exceptionally high chemical stability in a drastic medium such as in conc. H<sub>2</sub>SO<sub>4</sub> (36 N). The DFT calculations reveal that the presence of significant numbers of interlayer C–H⋯N H-bonding<sup>8</sup> between the methoxy (–OCH<sub>3</sub>) C–H of a particular layer with the imine (–C=N) nitrogen atoms present in the adjacent layers induces this exceptional

chemical stability within these frameworks. This interlayer C-H...N H-bonding improves interlayer stacking interaction and provides enough steric hindrance and hydrophobic crowding around the imine bonds and protects it from being hydrolyzed in such abrasive environment. Moreover, these COFs were further converted into self-standing and crack-free COF membranes (COFMs),<sup>5</sup> which maintain their physical appearance even after treatment with 18 N sulfuric acid solution for several days. These COFMs have been used to separate various environmentally toxic materials from drinking water. Apart from that, the as synthesized membranes showcased promising solvent flux specifically for acetone and acetonitrile, which are one of the highest values reported in the literature.

## Experimental Section

**General Synthetic Procedure:** All the COFs reported in this paper have been synthesized by reacting 2,4,6-trimethoxy-1,3,5-benzenetricarbonyldehyde (TpOMe) separately with 1,3,5-(4-aminophenyl) benzene (Tab), 1,4-phenylenediamine (Pa1), 2-nitro-1,4-phenylenediamine (PaNO<sub>2</sub>), 3,3'-dinitrobenzidine (BD(NO<sub>2</sub>)<sub>2</sub>), 4,4'-diamino-2,2'-bipyridine (BPy) and 4,4'-azodianiline (Azo) using *p*-toluenesulfonic acid (PTSA) as a molecular organizer as well as a water reservoir during the crystallization process (Figure 1). At first, PTSA-H<sub>2</sub>O (1.8 mmol) was mixed separately with respective amines in a mortar-pestle with subsequent addition of 1,3,5-Trimethoxy-2,4,6-benzenetricarbonyldehyde (TpOMe) (0.3 mmol) to this mixture, was followed by the addition of few drops of water (~100  $\mu$ L) based on requirement. The mixture was then appropriately grinded until it becomes dough like material. This dough like material was heated at 120 °C for 3h (or 90 °C for 12-24h). After completion, the resulting material was washed with water, *N,N*-dimethylacetamide (DMAc) and acetone, to afford crystalline porous COFs (~75-85% isolated yield). Additionally, to convert the COFs into the self-standing membrane, the soft dough material was moulded into proper geometrical shapes (here thin circular pattern) with 1cm diameter before heating at 60 °C (48 h), followed by 90 °C (6 h) (Section S-2, SI).

**Solvent flux measurements:** The solvent permeations were carried out using as-synthesized membrane coupons having 1 cm diameter and ~320  $\mu$ m thickness. The membranes were properly fitted on a dead-end-mode stirred cell (active area cal. 2.5 cm<sup>2</sup>) pressurized under 1 atm upstream pressure. The solvent flux was calculated based on the average of triplicate data's found for three different coupons. By measuring the permeate volume (V), the following equation was used to determine the solvent flux (J) per unit area (A) and per unit time (t):

$$J = V/(A.t)$$

In liters per square meter hour (Lm<sup>-2</sup>h<sup>-1</sup>). Overall permeance was calculated based on the equation  $P = V/(A.t \Delta p)$  in liters per square meter hour bar (Lm<sup>-2</sup>h<sup>-1</sup>bar<sup>-1</sup>) (Section S-10, SI).

**Rejection analysis:** Dye rejection was conducted by passing 100  $\mu$ M solutions of various dyes through the COF coupons under 1 bar pressure. Firstly, 2 ml of the filtrate was thrown out and about 5 ml of the same was collected for further rejection analyses. The particular dye concentration in feed and in permeate was determined using a double beam UV-Vis spectrometer. The percent rejection (%R) was calculated according to the equation:

$$\%R = [1 - (C_p/C_f)] \times 100$$

Where C<sub>p</sub> is the permeate concentration and C<sub>f</sub> is the feed concentration. The rejection values were calculated in case of rhodamine b (99.4%), rose Bengal dye (99.9%), methylene blue (99.9%) and congo

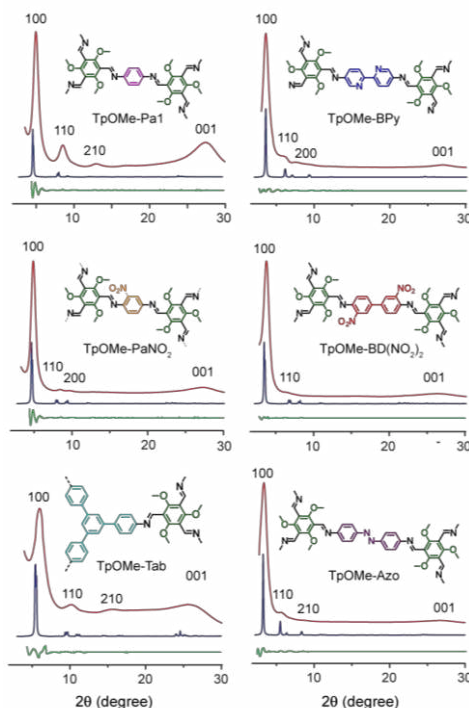


**Figure 2.** Comparison between experimental PXRD patterns (red) with simulated eclipsed stacking model (blue) along with their Pawley refinement difference (green) for all the COFs (Intensity shown in arbitrary unit). Partial chemdraw structures of respective COFs have shown on top of the PXRD patterns.

red (99.9%) (Section S-10, SI).

## Result and Discussion

PTSA mediated solid-state mixing approach has opened up a new route for rapid and bulk scale production of highly crystalline porous COFs, along with a broad opportunity for easy processability of the synthesized material in desirable forms.<sup>5c</sup> However, the exploration of the PTSA mediated solid state mixing approach is not straight forward for the construction of imine linked COFs. The primary concern is the chemical stability of the as synthesized frameworks under given reaction condition. Owing to intense acidic nature of PTSA ( $pK_a = -2.8$ ; Water), the imine-linked COF crystallites, during the framework formation, readily decompose under this experimental conditions leading to high extent of amorphization (Section S-7, SI). This makes it profoundly challenging to design suitable linker units, to yield the COFs with high chemical stability under the aforementioned synthetic conditions. We made a prediction that the synthesis of imine-linked COFs using this approach can only be achieved by providing enough steric hindrance around the imine bonds or by incorporating the significant hydrophobic crowding to protect it from H<sup>+</sup> and H<sub>2</sub>O attack during the COF crystallization under the aforementioned experimental condition.

The formation of TpOMe-Tab, TpOMe-PaNO<sub>2</sub>, TpOMe-Pa1, TpOMe-BD(NO<sub>2</sub>)<sub>2</sub>, TpOMe-BPy and TpOMe-Azo was confirmed

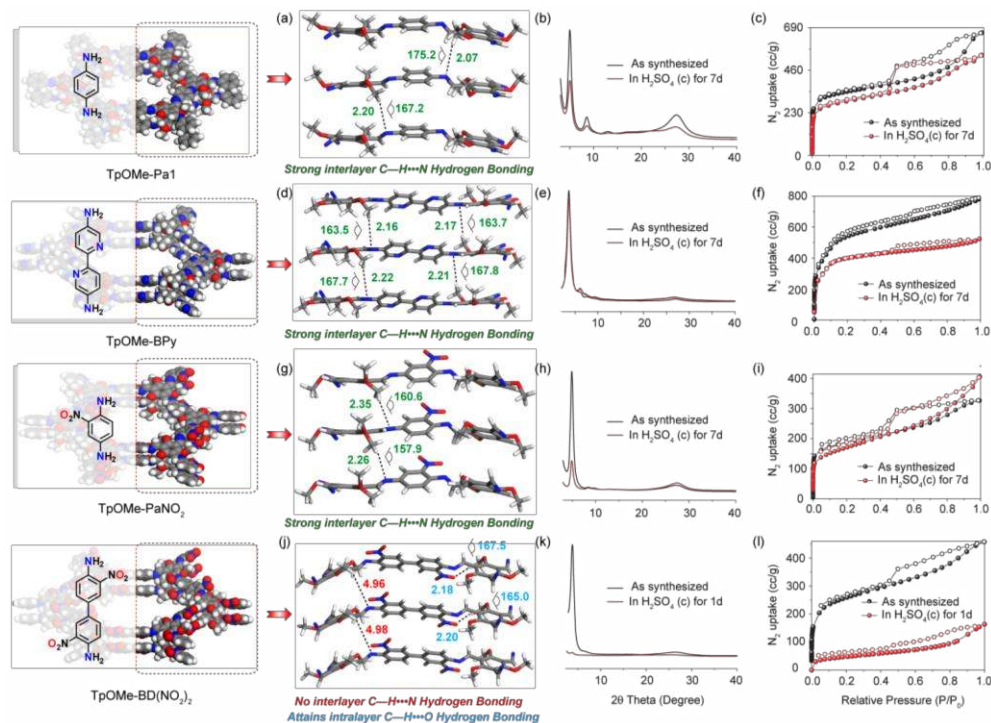


**Figure 3.** (a, d, g, and j) The layered structures of **TpOMe-Pa1**, **TpOMe-BPy**, **TpOMe-PaNO<sub>2</sub>** and **TpOMe-BD(NO<sub>2</sub>)<sub>2</sub>** (C-grey, N-blue, O-red and H-white). The interlayer C—H...N H-bonding based on distances (H to N atom; Å) shown with dotted line and angles (C—H...N) in degree (value assigned in green-within the range, red-outside the range). (b, e, and h) PXRD patterns and (c, f, and i) N<sub>2</sub> adsorption isotherms for **TpOMe-Pa1**, **TpOMe-BPy**, and **TpOMe-PaNO<sub>2</sub>** COFs, before and after treatment in H<sub>2</sub>SO<sub>4</sub> (36 N) for one week. (k) PXRD pattern and (l) N<sub>2</sub> adsorption isotherms for **TpOMe-BD(NO<sub>2</sub>)<sub>2</sub>** of as-synthesized and in H<sub>2</sub>SO<sub>4</sub> (c) for one day.

from their PXRD patterns (Figure 2). All the COFs mainly showed distinct peaks corresponding to the 100, 110 and 001 planes in their PXRD patterns. The high intense peak at  $\sim 4.8^\circ$  ( $\pm 0.1$ ,  $2\theta$ ), for **TpOMe-Pa1** and **TpOMe-PaNO<sub>2</sub>** COFs could be assigned to the reflections from its 100 planes. In case of **TpOMe-BD(NO<sub>2</sub>)<sub>2</sub>** and **TpOMe-BPy** high intense peaks attributed to 100 planes arise at  $\sim 3.6^\circ$  ( $\pm 0.1$ ,  $2\theta$ ). The **TpOMe-Azo** (with highest pore diameter in the series) and **TpOMe-Tab** (having lowest pore diameter) show their 100 plane reflections at  $\sim 3.3^\circ$  ( $2\theta$ ) and  $\sim 6.1^\circ$  ( $2\theta$ ), respectively. The high intensity of 100 planes in all the COFs indicates their high crystalline nature. All the COFs reveal their 001 plane reflections at  $\sim 27.1^\circ$  ( $\pm 0.2$ ,  $2\theta$ ) in the PXRD patterns. To find the inter layer stacking constitutions; two different model (eclipsed and staggered) structures were simulated by using Materials studio (Section S-4, ESI).<sup>12</sup> The experimental PXRD pattern fits well [**TpOMe-Tab** ( $R_p = 0.9\%$ ,  $R_{wp} = 1.8\%$ ); **TpOMe-PaNO<sub>2</sub>** ( $R_p = 2.7\%$ ,  $R_{wp} = 4.2\%$ ); **TpOMe-Pa1** ( $R_p = 2.3\%$ ,  $R_{wp} = 3.5\%$ ); **TpOMe-BD(NO<sub>2</sub>)<sub>2</sub>** ( $R_p = 0.7\%$ ,  $R_{wp} = 1.0\%$ ); **TpOMe-BPy** ( $R_p = 1.5\%$ ,  $R_{wp} = 2.4\%$ ) and **TpOMe-Azo** ( $R_p = 2.1\%$ ,  $R_{wp} = 2.9\%$ )] with the simulated slipped eclipsed (AA) stacking models. The unit cell parameters of the synthesized COFs were further evaluated using Pawley refinement of experimental PXRD patterns (Section S-4, SI).

The recorded FTIR spectra showed the complete disappearance of primary —N—H stretching frequency ( $3188\text{--}3462\text{ cm}^{-1}$ ) of parent amines as well as the —C=O stretching frequency at  $1682\text{ cm}^{-1}$  for the TpOMe aldehyde used for the synthesis in all COFs reported in this paper (Section S-5, SI). The newly formed —C=N bonds (obtained after aldehyde-amine Schiff base reaction) exhibit stretching frequency in the range of  $1574\text{--}1623\text{ cm}^{-1}$ , confirming the formation of imine bonds in the COFs and the full consumption of the starting materials. The synthesized reference compound **TpOMe-Ani** (prepared from TpOMe aldehyde with aniline) reflects —C=N stretching at  $\sim 1621\text{ cm}^{-1}$  (Section S-2, SI). The aromatic C=C stretching arises around  $\sim 1560\text{ cm}^{-1}$  (asymmetric) and  $\sim 1498\text{ cm}^{-1}$  (symmetric) in the FTIR spectra in all the COFs. The reference compound shows the similar stretching frequency  $\sim 1555$  and  $1483\text{ cm}^{-1}$ , respectively. The overall compositions of the framework materials were further confirmed from solid state <sup>13</sup>C cross-polarization/magic-angle spinning (CP-MAS) spectra, which reveal the main characteristics peak of imine (—C=N—) bonded carbon atom at  $\sim 148\text{ ppm}$  whereas the aromatic carbons show their

characteristic signals within the range ~53-70 ppm (Section S-5, SI). Similarly, the reference compound **TpOMe-Ani** exhibits the characteristics imine and aromatic carbon signals at ~163 ppm and ~150-115 ppm, respectively. Again, for **TpOMe-Ani** the signature of methoxy (-OCH<sub>3</sub>) carbon peak was observed at ~63 ppm, almost matching with the methoxy (-OCH<sub>3</sub>) carbon signals at reported COFs (Section S-2, SI).

The permanent porosity of any porous material imparts crucial information about the internal ordering of pores in that particular material. This information is highly essential in membrane based separation technologies. Hence, to evaluate the overall porosity of these COF materials reported in this paper, N<sub>2</sub> adsorption isotherms were recorded at 77 K (liq. N<sub>2</sub> temperature) in their completely activated state i.e. after treating the samples under vacuum (< 1 torr pressure) and heating at 150 °C for 12h. All the COFs show rapid N<sub>2</sub> uptake at comparatively lower pressure range P/P<sub>0</sub><0.1. Beyond this pressure, in case of **TpOMe-Tab**, **TpOMe-PaNO<sub>2</sub>**, **TpOMe-Pa1** and **TpOMe-BD(NO<sub>2</sub>)<sub>2</sub>** COFs, the isotherms get almost saturated, reflecting their dominating microporous nature (Figure 3, Section S-6, SI). **TpOMe-BPy** and **TpOMe-Azo**, on the other hand, show a sharp steep between the pressure P/P<sub>0</sub>= 0.10-0.20, exhibiting the 'type-IV' adsorption isotherm, which is the characteristic of mesoporous materials (Figure 3, Section S-6, SI). Moreover, based on Brunauer–Emmett–Teller (BET) model **TpOMe-BPy** reveals a highest surface area of 2023 m<sup>2</sup>g<sup>-1</sup>, followed by 1885 m<sup>2</sup>g<sup>-1</sup> for **TpOMe-Azo**, 1164 m<sup>2</sup>g<sup>-1</sup> for **TpOMe-Pa1**, 913 m<sup>2</sup>g<sup>-1</sup> for **TpOMe-BD(NO<sub>2</sub>)<sub>2</sub>**, 615 m<sup>2</sup>g<sup>-1</sup> for **TpOMe-PaNO<sub>2</sub>** and 593 m<sup>2</sup>g<sup>-1</sup> for **TpOMe-Tab**. The experimental pore size distribution of **TpOMe-Tab**, **TpOMe-PaNO<sub>2</sub>**, **TpOMe-Pa1** and **TpOMe-BD(NO<sub>2</sub>)<sub>2</sub>** COFs (calculated using QSDFT model: cylindr. pore, adsorption branch), show the pore width as 1.4, 1.4, 1.5 and 1.8 nm respectively (Section S-6, ESI). The pore diameter for **TpOMe-BPy** and **TpOMe-Azo** was determined as 2.2 and 2.8 nm (Section S-6, SI). Interestingly, we have tested these COFs for CO<sub>2</sub> uptake both at 0 and 25 °C where **TpOMe-Azo** shows highest CO<sub>2</sub> uptake of 87ccg<sup>-1</sup> at 0 °C (Section S-6, SI). Thermogravimetric analyses (TGA) (N<sub>2</sub> atmosphere) of all the COFs shows their thermal stability in the range 320-400 °C (Section S-5, SI). However, **TpOMe-PaNO<sub>2</sub>** and **TpOMe-BD(NO<sub>2</sub>)<sub>2</sub>** show rapid weight loss (100 to almost 0 %) within 330-340 °C. **TpOMe-Pa1** showcased highest thermal stability in the series reflecting only 30 % weight loss even after treated up to 900 °C.

The extent of chemical stability of any material dictates its potentiality for extensive usage. Hence, to analyze the chemical stability here, the as-synthesized COF samples (30 mg) were submerged in different types of solvents (3 ml) for 7 days. The chemical stability of the COFs was carried out in highly drastic mediums such as conc. H<sub>2</sub>SO<sub>4</sub> (36 N), conc. HCl (12 N), NaOH (9 N, 24 h) and various protic/aprotic solvents including H<sub>2</sub>O (boiling), acetone, EtOH, MeOH, CH<sub>3</sub>CN, *N,N*-Dimethylformamide (DMF), Dimethylsulfoxide (DMSO), Dichloromethane (DCM) and Chloroform (CHCl<sub>3</sub>) (Section S-6, SI). After the treatment, the material was collected and was washed thoroughly with water, DMAc followed by acetone, before it was vacuum dried to remove the trapped solvent molecules. All the COFs reported here exhibit almost no weight loss (<0.1 wt.%) in water and other protic or aprotic solvents. Except for **TpOMe-BD(NO<sub>2</sub>)<sub>2</sub>**, other COFs maintain the residual weight percentage in the range 70-75 and 80-90 wt % after seven days treatment in an ultra-abrasive environment such as in conc. H<sub>2</sub>SO<sub>4</sub> (36 N) and conc. HCl (12 N) respectively. Whereas, on an average 50-60 wt% is retained for respective COFs after treatment in NaOH (9N) for 24 h. **TpOMe-BD(NO<sub>2</sub>)<sub>2</sub>** was found to be highly sensitive towards conc. H<sub>2</sub>SO<sub>4</sub> (36 N) and NaOH (9 N) (<24

hours but found to be stable in HCl (12 N) for 7 days.(Figure 3k & l; Section S-6, SI). The proper matching in the PXRD patterns, along with their comparatively identical FTIR spectra, concerning as-synthesized materials revealed their structural rigidity almost in every medium (Section S-6, ESI). N<sub>2</sub> adsorption isotherms revealed that the acid, water, and organic solvent treated COFs maintain their porosity. The BET surface areas observed for **TpOMe-BPy** (1512, 1844 and 689 m<sup>2</sup>g<sup>-1</sup>), **TpOMe-Azo** (1527, 1805 and 1469 m<sup>2</sup>g<sup>-1</sup>), **TpOMe-Pa1** (1014, 1112, 780 m<sup>2</sup>g<sup>-1</sup>), **TpOMe-BD(NO<sub>2</sub>)<sub>2</sub>** (170, 770 and 0 m<sup>2</sup>g<sup>-1</sup>), **TpOMe-PaNO<sub>2</sub>** (603, 612 and 206 m<sup>2</sup>g<sup>-1</sup>) and **TpOMe-Tab** (584, 590 and 104 m<sup>2</sup>g<sup>-1</sup>) after treating the respective COF samples in conc. H<sub>2</sub>SO<sub>4</sub> (36 N, seven days), conc. HCl (12 N, seven days) and NaOH (9 N, 24h) respectively.

Density Functional Tight Binding (DFTB) and Density Functional Theory (DFT) calculations were undertaken taken into consideration to gain more insights about this exceptionally high chemical stability of the COFs. Interestingly, it was observed that the methoxy (-OCH<sub>3</sub>) groups present in the aldehyde subunits play a very crucial role in stabilizing these materials. However, their ~~absence~~ presence does not impart the stability. The methoxy (-OCH<sub>3</sub>) groups present in the COFs, except **TpOMe-BD(NO<sub>2</sub>)<sub>2</sub>**, were almost perpendicularly directed into the interlayer spacing in all the structures (Figure 3a, d & g; Section S-7, SI). As a result, a significant number (6-12 H-bonding per hexagonal bilayer) of interlayer C-H...N H-bonding interactions were discerned between the methoxy (-OCH<sub>3</sub>) C-H of a particular layer and imine (C=N) nitrogen atom present in the adjacent layer. The calculated H-bonding distances in slipped-AA structures for **TpOMe-Pa1** [D=3.17 Å, d=2.07 Å, θ=175.2°], **TpOMe-PaNO<sub>2</sub>** [D=3.31 Å, d=2.26 Å, θ=157.9°], **TpOMe-Tab** [D=3.24 Å, d=2.17 Å, θ=160.4°], **TpOMe-BPy** [D=3.24 Å, d=2.16 Å, θ=163.5°], **TpOMe-Azo** [D=3.24 Å, d=2.15 Å, θ=166.3°] suggest the existence of C-H...NH-bonding interactions in these COFs. The calculated distances are within the range of strong C-H...N (d≤2.7 Å, θ≥150°) H-bonding interactions,<sup>8a</sup> thereby providing additional strength during the stacking of layers. However, in case of **TpOMe-BD(NO<sub>2</sub>)<sub>2</sub>**, the methoxy (-OCH<sub>3</sub>) groups mainly lie in the plane of the aldehyde phenyl ring, due to the presence of intra-layer C-H...O [D=3.27 Å, d=2.18 Å, θ=167.5°]; H-bonding between methoxy (-OCH<sub>3</sub>) C-H of the aldehyde and nitro (-NO<sub>2</sub>) oxygen atoms of BD(NO<sub>2</sub>)<sub>2</sub> amine (Figure 3j). As a result, **TpOMe-BD(NO<sub>2</sub>)<sub>2</sub>** lacks such interlayer C-H...N H-bonding, rather it maintains only intralayer C-H...O H-bonding. Hence, the imine (C=N) bonds, which are devoid of such stabilizing H-bonding gets disrupted via the rapid attack from H<sup>+</sup> or OH<sup>-</sup>, signifying the lower chemical stability of **TpOMe-BD(NO<sub>2</sub>)<sub>2</sub>** (Section S-6, SI).

Furthermore, the plausible reason for the comparatively less chemical stability of COFs in strong base (OH<sup>-</sup>) compared to strong acids (H<sup>+</sup>) could be realized via examining the acid-base hydrolysis mechanism of imine (C=N) bond (Section S-6, SI). In **TpOMe-X** (X= **Tab**, **PaNO<sub>2</sub>**, **Pa1**, **BPy** and **Azo**) COFs the existing interlayer C-H...N H-bonding interactions minimize the lone pair availability on the imine 'N' atom thereby reducing their protonation tendency which is a key initiative of hydrolysis in acid medium (Figure S19). On the other hand base mediated hydrolysis is triggered by the nucleophilic attack of the hydroxide (OH<sup>-</sup>) ion on the imine (C=N) 'C' atom, which is free and much accessible, to carry forward the rest of the hydrolysis steps in basic medium (Figure S20).

Again, to address the precise role of the methoxy (-OCH<sub>3</sub>) group in stability, we have calculated the π-π stacking energy between two

Formatted: Highlight

Formatted: Highlight

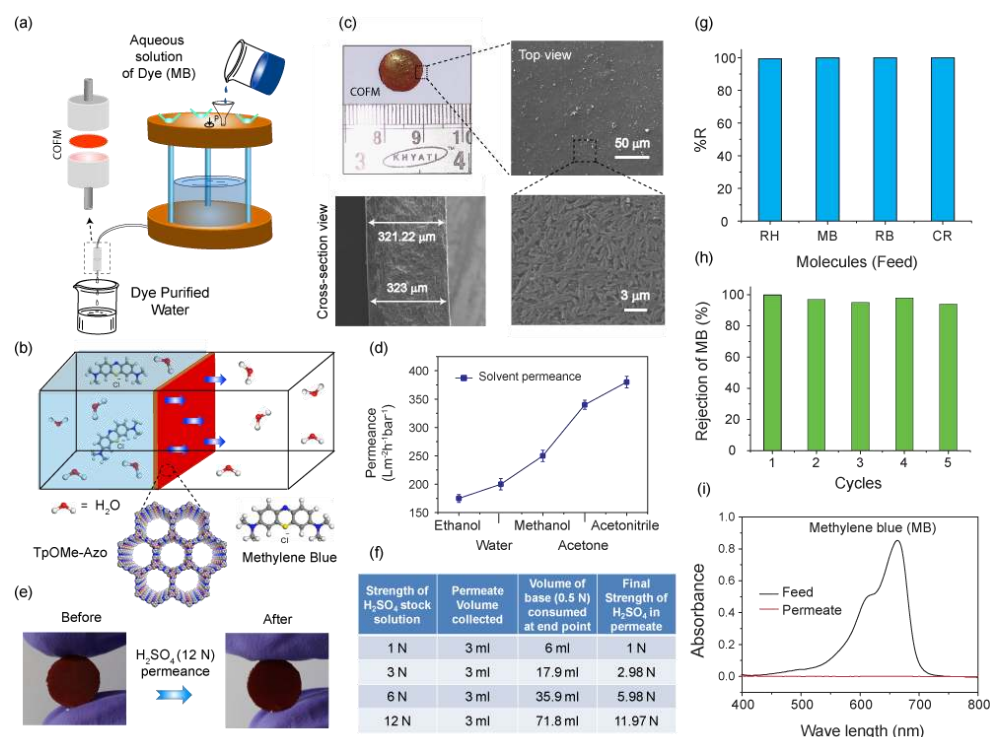


**Figure 4:** Application of COF membranes (COFMs) in waste water treatment via the nano-filtration process. (a) Schematic illustration of the nano-filtration assembly showing water purification process from organic dyes (MB- Methylene Blue). (b) Schematic representation of the selective separation through ordered pore structure of **TpOMe-Azo** COFM. (c) SEM images of COFM (top and cross section view as shown). (d) Pure solvent permeance study for **TpOMe-Azo** COFM. (e) Physical appearance of the membrane before and after 12 (N) sulfuric acid permeation. (f) Tabular representation for a quantitative test for a proton in permeate through titration test with standard aq. NaOH base. (g) Membrane based rejection analysis of various dyes from water. (h) Recyclability test of the **TpOMe-Azo** membrane for Methylene Blue (MB) for consecutive five cycles. (i) UV-Vis spectrum comparison for Methylene Blue feed.

stacked hexagons. First, we have investigated and compared the crystal stacking energy of TpOMe-COFs and COFs lacking such methoxy groups i.e. Tf-COFs (COFs constructed from 1,3,5-benzenetricarbaldehyde (Tf) with all six amines reported in this paper) (Section S-7, SI). The calculated relative energies (KJ/mole) for TpOMe-Tab (-1072.4) and Tf-Tab (-993.1); TpOMe-PaNO<sub>2</sub> (-1560.8) and Tf-PaNO<sub>2</sub> (-1337.53); TpOMe-Pa1 (-1332.2) and Tf-Pa1 (-1099.5); TpOMe-BD(NO<sub>2</sub>)<sub>2</sub> (-2211.6) and Tf-BD(NO<sub>2</sub>)<sub>2</sub> (-1850.6); TpOMe-BPy (-1672.9) and Tf-BPy (-1274.5); TpOMe-Azo (-1747.7) and Tf-Azo (-1362.2) suggest the probable reason of the high stability for TpOMe-COFs. We believe that, much negative crystal stacking energy implies the greater stability of TpOMe-COFs over Tf-COFs, and also manifests the limitation for their (Tf-COFs) production using PTSA based solid state mixing method (Section S-7, SI). Moreover, among the methoxy functionalized COFs **TpOMe-BD(NO<sub>2</sub>)<sub>2</sub>** showcased most negative crystal stacking energy (-2211.6 KJ/mole), hence signifying foremost interlayer stacking interaction. But, in contrary, **TpOMe-BD(NO<sub>2</sub>)<sub>2</sub>** conveys least chemical stability as seen from the chemical stability experiments in harsh conditions, and certainly the reason would be the absence of such interlayer H-bonding in **TpOMe-BD(NO<sub>2</sub>)<sub>2</sub>**. Hence, the overall findings evidently indicate the remarkable chemical stability of

these materials doesn't depend upon simply placing methoxy (-OMe) functionality in the frameworks; moreover it mainly relies on the presence of such stabilizing interlayer H-bonding.

We carried out time dependent morphological evolution<sup>9</sup> studies using electron microscopic analysis of **TpOMe-Pa1** particles, to obtain insight into the overall crystallization process during this solid state synthesis of the COFs reported in this paper (Section S-8, SI).<sup>10</sup> Both SEM and TEM imaging exhibits that at lower reaction time (0-15 min), the COF particles form dis-oriented small fibrous crystallites. At 30 min of reaction time, the number of scattered fibers starts reducing and they connect each other laterally to grow in two dimensions to form large sheets. After 45-60 min, it was observed that the significantly bigger crystallites composed from nicely packed sheets in the perpendicular direction is formed, along with the complete disappearance of fibers. After 3h of reaction time, count of such crystallites increases and no more change in morphology was observed from SEM or TEM analyses, suggesting the completion of overall morphological evolution (Section S-8, SI).

Since the as-synthesized COFs were stable at extreme conditions, we have decided to fabricate the chemically stable membranes by merely moulding the dough material into proper geometrical shapes. Owing to its comparatively easy route of process-

ability and high crystalline nature, self-standing **TpOMe-Azo** COF membranes (COFMs) has been synthesized. This as-synthesized defect-free membrane exhibits high crystallinity and porosity similar to parent COF. SEM images (top view) show that the membranes are composed of  $\sim 1\text{--}3\ \mu\text{M}$  crystallites, which are perfectly packed with each other (**Figure 4c**; **Section S-9, SI**). As shown in **Figure 4c**, the thickness of the membrane calculated from its cross section SEM analysis was around  $320\ \mu\text{M}$ . The thickness of membranes can be tuned depending on the proper choice of mould thickness and can be varied from  $200\ \mu\text{M}$  to any upper value based on requirement (**Section S-9, SI**). A coupon of  $1\ \text{cm}$  diameter and  $\sim 320\ \mu\text{M}$  thickness was submerged in  $10\ \text{ml}$  of solvent (water, acetone, acetonitrile, methanol and ethanol) and  $18\ \text{N}$  sulphuric acid solutions, for three days to address the chemical stability of the membrane. The negligible swelling nature ( $<1\%$ ) and same physical appearance observed for the membranes demonstrated the structural integrity of the membrane in every medium. The detailed structural investigations using PXRD, FT-IR,  $\text{N}_2$  adsorption and SEM imaging of the chemically treated membranes reflect no alteration in the underlying framework structure (**Section S-9, SI**).

We have utilized this COF as the high-performance separation membranes in drastic environment, where toxic solvents or highly acidic solution are involved (**Figure 4a & b**). The COF showed considerably high solvent flux for acetonitrile ( $380\ \text{L m}^{-2}\text{h}^{-1}\text{bar}^{-1}$ ), followed by acetone ( $340\ \text{L m}^{-2}\text{h}^{-1}\text{bar}^{-1}$ ), methanol ( $250\ \text{L m}^{-2}\text{h}^{-1}\text{bar}^{-1}$ ), water ( $200\ \text{L m}^{-2}\text{h}^{-1}\text{bar}^{-1}$ ) and ethanol ( $175\ \text{L m}^{-2}\text{h}^{-1}\text{bar}^{-1}$ ), reflecting its potentiality towards waste solvent treatment (**Figure 4d**; **Section S-10, SI**). Sulphuric acid is industrially used and highly important manufactured chemical by many industries, not only due to its usability in various reactions, but also due to its high reactivity. Although many methods have been demonstrated for its decomposition after reaction, very few attempts have been done for its recovery from the reaction mixture.<sup>11</sup> In these circumstances, we believe that sulfuric acid purification *via* membrane permeance could be another route for its recovery process. Considering the high chemical stability of as-synthesized **TpOMe-Azo** membrane, we have tested the same for standard sulphuric acid solution permeance. Initially, we passed different aqueous solution of  $\text{H}_2\text{SO}_4$  with a concentration of  $1\ \text{N}$ ,  $3\ \text{N}$ ,  $6\ \text{N}$  and  $12\ \text{N}$  through the membrane to analyse its permeance performance, where we observed the as high as  $> 99\%$  permeance (**Figure 4f**). The physical appearance of the membrane was significantly intact reflecting its robustness during the process (**Figure 4e**). Every time, the strength of the eluted sulphuric acid solution was estimated *via* titration with standard aqueous sodium hydroxide ( $0.5\ \text{N}$ ) using phenolphthalein as an acid-base titration indicator. By measuring the volume of the base consumed at the end point, the final strength of sulphuric acid was calculated, which reflects the negligible change in the concentration in the elute compared to the stock solution (**Figure 4f**). Furthermore, the COFMs were further utilized for challenging separations of expensive ingredients like methylene blue, dye molecules such as rhodamin b, rose Bengal and congo red, from the drinking water with high recyclability (**Figure 4g & h**). The rejection performance of the COF was realized from UV-Vis spectra of permeate by comparing with its mother feed solution. From these UV-Vis analyses, complete disappearance of the main characteristics absorption peaks in the range  $500\text{--}700\ \text{nm}$  has been observed for the permeate, signifying for all the dyes with  $> 99\%$  rejection (**Figure 4i**; **Section S-10, SI**). The high rejection capability for broad range of water contaminants further suggests the applications of COFMs for water purification technologies.

## Conclusions

In summary, we have designed and synthesized a series of imine ( $\text{--C=N--}$ ) linked porous and crystalline COFs *via* salt (*p*-toluenesulfonic acid- $\text{H}_2\text{O}$ ) mediated crystallization process. This preferred approach is economically beneficial as it provides a very simple route for rapid and bulk scale production of the incredibly versatile imine-based COFs, with high crystallinity and porosity. The as-synthesized materials showcased ultra-high chemical stability in extremely drastic mediums such as strong acids (conc.  $\text{H}_2\text{SO}_4$  and  $\text{HCl}$ ; seven days) and base ( $\text{NaOH}$ ,  $9\ \text{N}$ ;  $24\ \text{h}$ ). DFT calculations of the structures revealed that the presence of inter-layer H-bonding is mainly responsible for the ultrahigh stability of these materials, as it strengthened the layers stacking and protects the imine bond from hydrolysis *via* providing enough steric hindrance and hydrophobic environments. The COFs were further transformed to self-standing, continuous and defect-free Covalent Organic Framework Membranes (COFMs) with significant crystallinity and porosity, along with considerable chemical stability. These as-synthesized COFMs are highly useful for the purification of sulphuric acid, and removal of toxic substances and organic carcinogenic dyes from water. In these circumstances, we believe that PTSA based solid state synthesis could serve as a benchmark for this multifaceted imine COF synthesis not only due to its greener synthesis conditions and bulk scale productivity, but also due to the processability of COFs in desirable forms. The easy and large-scale production of COFs and COFMs using this approach may pave its future applications in water purification technologies.

## ASSOCIATED CONTENT

### Supporting Information

Synthetic procedures, PXRD, Gas Adsorption, FT-IR,  $^{13}\text{C}$  solid state NMR, TGA, SEM, TEM, crystallographic data (CIF), theoretical details. This material is available free of charge via the Internet at <http://pubs.acs.org>.

## AUTHOR INFORMATION

### Corresponding Author

r.banerjee@ncl.res.in

### Notes

The authors declare no competing financial interests.

## ACKNOWLEDGMENT

AH and SB acknowledge CSIR, SK acknowledge UGC, India for research fellowships. We acknowledge Dr. Amit Chakrabarty and Himadri Sekhar Sasmal for single crystal data collection. R.B. acknowledges DST Indo-Singapore Project (INT/SIN/P-05) and DST Nanomission Project (SR/NM/NS-1179/2012 G) for funding. We acknowledge Dr. T. G. Ajithkumar and Anjali Krishna M. for the NMR facility; Dr. C. Ramesh and Dr. Guruswamy K. for the PXRD facility.

## REFERENCES:

- (a) Uribe-Romo, F. J.; Hunt, J. R.; Furukawa, H.; Klöck, C.; O'Keeffe, M.; Yaghi, O. M. *J. Am. Chem. Soc.* **2009**, *131*, 4570. (b) Han, X.; Xia, Q.; Huang, J.; Liu, Y.; Tan, C.; Cui, Y. *J. Am. Chem. Soc.* **2017**, *139*, 8693. (c) Liu, X.-H.; Guan, C.-Z.; Ding, S.-Y.; Wang, W.; Yan, H.-J.; Wang, D.; Wan, L.-J. *J. Am. Chem. Soc.* **2013**, *135*, 10470. (d) Ding, S.-Y.; Wang, W. *Chem. Soc. Rev.* **2013**, *42*, 548. (e) Sun, A.; Aguila, B.; Perman, J.; Nguyen, N.; Ma, S. *J. Am. Chem.*

- Soc. **2016**, *138*, 15790. (f) Crowe, J. W.; Baldwin, L. A.; McGrier, P. L. *J. Am. Chem. Soc.* **2016**, *138*, 10120. (g) Pang, S. F.; Xu, S. Q.; Zhou, T. Y.; Liang, R. R.; Zhan, T. G.; Zhao, X. *J. Am. Chem. Soc.* **2016**, *138*, 4710. (h) Kuhn, P.; Antonietti, M.; Thomas, A. *Angew. Chem., Int. Ed.* **2008**, *47*, 3450. (i) Zhang, Y.; Duan, J.; Ma, D.; Li, P.; Li, S.; Li, H.; Zhou, J.; Ma, X.; Feng, X.; Wang, B. *Angew. Chem., Int. Ed.* **2017**, *56*, 16313.
2. (a) Ding, H.; Li, Y.; Hu, H.; Sun, Y.; Wang, J.; Wang, C.; Wang, C.; Zhang, G.; Wang, B.; Xu, W.; Zhang, D. *Chem. - Eur. J.* **2014**, *20*, 14614. (b) Rambo, B. M.; Lavigne, J. J. *Chem. Mater.*, **2007**, *19*, 3732. (c) Stegbauer, L.; Schwinghammer, K.; Lotsch, B. V. *Chem. Sci.* **2014**, *5*, 2789. (d) Doonan, C. J.; Tranchemontagne, D. J.; Glover, T. G.; Hunt, J. R.; Yaghi, O. M. *Nat. Chem.* **2010**, *2*, 235. (e) Ascherl, L.; Sick, T.; Margraf, J. T.; Lapidus, S. H.; Calik, M.; Hettstedt, C.; Karaghiosoff, K.; Döblinger, M.; Clark, T.; Chapman, K. W.; Auras, F.; Bein, T. *Nat. Chem.* **2016**, *8*, 310. (f) Ding, S. Y.; Gao, J.; Wang, Q.; Zhang, Y.; Song, W. G.; Su, C. Y.; Wang, W. J. *Am. Chem. Soc.* **2011**, *133*, 19816. (g) Qian, C.; Xu, S.-Q.; Jiang, G.-F.; Zhan, T.-G.; Zhao, X. *Chem. - Eur. J.* **2016**, *22*, 17784.
3. (a) Lanni, L. M.; Tilford, R. W.; Bharathy, M.; Lavigne, J. J. *J. Am. Chem. Soc.*, **2011**, *133*, 13975. (b) Rabbani, M. G.; Sekizkardes, A. K.; Kahveci, Z.; Reich, T. E.; Ding, R.; El-Kaderi, H. M. *Chem. Eur. J.* **2013**, *19*, 3324. (c) Vyas, V. S.; Haase, F.; Stegbauer, L.; Savasci, G.; Podjaski, F.; Ochsenfeld, C.; Lotsch, B. V. *Nat. Commun.* **2015**, *6*, 8508. (d) Elsbahy, M.; Wooley, K. L. *Chem. Soc. Rev.* **2012**, *41*, 2545. (e) Vyas, V. S.; Vishwakarma, M.; Moudrakovski, I.; Haase, F.; Savasci, G.; Ochsenfeld, C.; Spatz, J. P.; Lotsch, B. V. *Adv. Mater.* **2016**, *28*, 8749. (f) Pachfule, P.; Kandambeth, S.; Díaz, D. D.; Banerjee, R. *Chem. Commun.*, **2014**, *50*, 3169. (g) Deblase, C. R.; Silberstein, K. E.; Truong, T.; Abruña, H. D.; Dichtel, W. R. *J. Am. Chem. Soc.* **2013**, *135*, 16821. (h) Ma, Y.-X.; Li, Z.-J.; Wei, L.; Ding, S.-Y.; Zhang, Y.-B.; Wang, W. J. *Am. Chem. Soc.* **2017**, *139*, 4995.
4. (a) Kandambeth, S.; Mallick, A.; Lukose, B.; Mane, M. V.; Heine, T.; Banerjee, R. *J. Am. Chem. Soc.* **2012**, *134*, 19524. (b) Waller, P. J.; Lyle, S. J.; Popp, T. M. O.; Diercks, C. S.; Reimer, J. A.; Yaghi, O. M. *J. Am. Chem. Soc.* **2016**, *138*, 15519. (c) Lanni, L. M.; Tilford, R. W.; Bharathy, M.; Lavigne, J. J. *J. Am. Chem. Soc.* **2011**, *133*, 13975. (d) Kandambeth, S.; Shinde, D. B.; Panda, M. K.; Lukose, B.; Heine, T.; Banerjee, R. *Angew. Chem., Int. Ed.* **2013**, *52*, 13052. (e) Du, Y.; Mao, K.; Kamakoti, P.; Pavikovitch, P.; Paur, C.; Cundy, S.; Li, Q.; Calabro, D. *Chem. Commun.* **2012**, *48*, 4606. (f) Xu, H.; Gao, J.; Jiang, D. *Nat. Chem.* **2015**, *7*, 905.
5. (a) Kandambeth, S.; Biswal, B. P.; Chaudhari, H. D.; Rout, K. C.; Kunjattu, H. S.; Mitra, S.; Karak, S.; Das, A.; Mukherjee, R.; Kharul, U. K.; Banerjee, R. *Adv. Mater.* **2017**, *29*, 1603945. (b) Karak, S.; Kandambeth, S.; Biswal, B. P.; Sasmal, H. S.; Kumar, S.; Pachfule, P.; Banerjee, R. *J. Am. Chem. Soc.* **2017**, *139*, 1856. (c) Dey, K.; Pal, M.; Rout, K. C.; Kunjattu, H. S.; Das, A.; Mukherjee, R.; Kharul, U. K.; Banerjee, R. *J. Am. Chem. Soc.*, **2017**, *139*, 13083.
6. (a) Segura, J. L.; Mancheño, M. J.; Zamora, F. *Chem. Soc. Rev.* **2016**, *45*, 5635. (b) Smith, B. J.; Overholts, A. C.; Hwang, N.; Dichtel, W. R. *Chem. Commun.* **2016**, *52*, 3690. (c) Schwab, M. G.; Hamburger, M.; Feng, X.; Shu, J.; Spiess, H. W.; Wang, X.; Antonietti, M.; Müllen, K. *Chem. Commun.* **2010**, *46*, 8932. (d) Halder, A.; Kandambeth, S.; Biswal, B. P.; Kaur, G.; Roy, N. C.; Addicoat, M.; Salunke, J. K.; Banerjee, S.; Vanka, K.; Heine, T.; Verma, S.; Banerjee, R. *Angew. Chem., Int. Ed.* **2016**, *55*, 7806.
7. (a) Biswal, B. P.; Chandra, S.; Kandambeth, S.; Lukose, B.; Heine, T.; Banerjee, R. *J. Am. Chem. Soc.* **2013**, *135*, 5328. (b) Matsumoto, M.; Dasari, R. R.; Ji, W.; Feriante, C. H.; Parker, T. C.; Marder, S. R.; Dichtel, W. R. *J. Am. Chem. Soc.* **2017**, *139*, 4999.
8. (a) Taylor, R.; Kennard, O. *J. Am. Chem. Soc.* **1982**, *104*, 5063. (b) Sarma, J. A. R. P.; Desiraju, G. R. *Acc. Chem. Res.*, **1986**, *19*, 222. (c) Desiraju, G. R. *Angew. Chem., Int. Ed. Engl.* **1995**, *34*, 2311. (d) Desiraju, G. R. *Acc. Chem. Res.*, **1996**, *29*, 441. (e) Desiraju, G. R. *Acc. Chem. Res.*, **2002**, *35*, 565. (f) Desiraju, G. R. *J. Am. Chem. Soc.* **2013**, *135*, 9952. (g) Desiraju, G. R.; Steiner, T. *The weak hydrogen bond in structural chemistry and biology*. Oxford University Press: Oxford, 1999.
9. (a) Chen, J. S.; Archer, L. A.; Lou, X. W.; *J. Mater. Chem.* **2011**, *21*, 9912. (b) Mahmoud, M. A.; Narayanan, R.; El-Sayed, M. A. *Acc. Chem. Res.* **2013**, *46*, 1795. (c) Jin, R.; Cao, Y.; Mirkin, C. A.; Kelly, K. L.; Schatz, G. C.; Zheng, J. G. *Science* **2001**, *294*, 1901. (d) Chen, Z.; Wang, H. I.; Teyssandier, J.; Mali, K. S.; Dumsclaff, T.; Ivanov, I.; Zhang, W.; Ruffieux, P.; Fasel, R.; Räder, H. J.; Turchinovich, D.; De Feyter, S.; Feng, X.; Kläui, M.; Narita, A.; Bonn, M.; Müllen, K. *J. Am. Chem. Soc.* **2017**, *139*, 3635. (e) Kandambeth, S.; Venkatesh, V.; Shinde, D. B.; Kumari, S.; Halder, A.; Verma, S.; Banerjee, R. *Nat. Commun.* **2015**, *6*, 6786. (f) Gole, B.; Stepanenko, V.; Rager, S.; Grüne, M.; Medina, D. D.; Bein, T.; Würthner, F.; Beuerle, F. *Angew. Chem., Int. Ed.* (DOI: 10.1002/anie.201708526)
10. Six different set of vials were kept in the oven after mixing the precursor materials (aldehyde, amine, PTSA and water), with the same concentration necessary for the TpOMe-Pa1 COF synthesis. The mixture was allowed to heat for 15 min, 30 min, 45 min, 1h, 2h and 3h at 120 °C, followed by cooling and quenching with addition of excessive water (to remove PTSA) and DMAc (to remove unreacted starting materials or polymeric impurities), along with acetone exchange prior to the drying. PXRD, FT-IR and N<sub>2</sub> adsorption analyses of the dry powder samples reveal that the COF formation happens even at smaller reaction time (within 15 min) (Section S-8, SI). The morphological change with time was investigated from Scanning Electron Microscopy (SEM) and Transmittance Electron Microscopy (TEM).
11. (a) Song, K.; Meng, Q. Q.; Shu, F.; Ye, Z. F. *Chemosphere* **2013**, *90* (4), 1558. (b) Bartholomew, F. J. *Ind. Eng. Chem.* **1952**, *44*, 541. (c) Li, G.; Asselin, E.; Li, Z. *Ind. Eng. Chem. Res.* **2014**, *53*, 11794. (d) Chairapat, S.; Wongchan, S.; Loykulnant, S.; Kongkaew, C.; Charnnok B. *Process Saf. Environ.* **2015**, *94*, 420. (e) Elkina, I. B.; Gilman, A. B.; Ugrosov, V. V.; Volkov V. V. *Ind. Eng. Chem. Res.*, **2013**, *52*, 8856.
12. Accelrys, Material Studio Release Notes, Release 4.2, Accelrys Software, San Diego 2006.